ADVANCED ENERGY MATERIALS
www.advenergymat.de

Design Principles for Cation-Mixed Sodium Solid Electrolytes

*Zhuoying Zhu, Hanmei Tang, Ji Qi, Xiang-Guo Li, and Shyue Ping Ong**

All-solid-state sodium-ion batteries are highly promising for next generation grid energy storage with improved safety. Among the known sodium superionic conductors, the Na_3PnS_4 family and the recently discovered $Na_{11}Sn_2PnS_{12}$ (Pn = P, Sb) have garnered major interest due to their extremely high ionic conductivities. In this work, comprehensive investigation of the Na_3PnS_4-Na_4TtS_4 (Pn = P/As/Sb, Tt = Si/Ge/Sn) phase space of superionic conductors using density functional theory calculations, as well as AIMD simulations on the promising new $Na_{11}Sn_2PnS_{12}$ (Pn=P/As/Sb) structures are presented. Crucial design rules on the effect of cation mixing are extracted on relative phase stability, electrochemical stability, moisture stability, and ionic conductivity. In particular, it is shown that while larger cations can substantially improve the ionic conductivity and moisture stability in these structures, there is an inherent trade-off in terms of electrochemical stability. $Na_{11}Sn_2AsS_{12}$ is also identified as a hitherto unexplored stable sodium superionic conductor with higher Na^+ conductivity and better moisture stability than the $Na_{11}Sn_2PS_{12}$ and $Na_{11}Sn_2SbS_{12}$ phases already reported experimentally.

1. Introduction

Rechargeable all-solid-state sodium-ion batteries utilizing a superionic conductor solid electrolyte (SE) have garnered substantial interest in recent years.[1–3] An all-solid-state architecture promises to be safer and potentially more energy dense, while the use of abundant and cheap sodium in place of lithium addresses potential concerns with regards to availability and cost, especially for larger scale applications. Furthermore, sodium-ion chemistry also opens up unexplored compositions and structural spaces that are not found in lithium-ion chemistry (e.g., P2 layered materials), which expands the scope for finding chemically and mechanically well-matched electrode-SE combinations.

Among the known sodium superionic conductors,[1–4] Na_3PS_4[5–7] and its derivatives have stood out due to their especially high ionic conductivities. With a high ionic conductivity (0.2 mS cm^{-1}) reported by Hayashi et al.[6] in 2012, intensive research has pushed its conductivity to above 1 mS cm^{-1} through aliovalent cation (e.g., P^{5+} for Sn^{4+})[8,9] and anion (e.g., S^{2-} for Cl^-)[10,11] doping as well as isovalent substitution of P for Sb/As.[12–16] In 2019, a 12% W^{6+} doping in cubic-Na_3SbS_4[17] achieved the highest conductivity (32 mS cm^{-1}) that ever reported. Recently, a new archetype has been discovered in the Na_3PnS_4-Na_4TtS_4 system with composition $Na_{11}Tt_2PnS_{12}$ (Pn = P/Sb, Tt = Sn) and a tetragonal $I4_1/acd$ space group.[18–20] $Na_{11}Sn_2PS_{12}$ have independently been reported by refs. [18] and [19] with ionic conductivities of 1.4–3.7 mS cm^{-1}, while $Na_{11}Sn_2SbS_{12}$ has also been reported by refs. [21] and [22] with ionic conductivities of 0.2–0.56 mS cm^{-1}. Jia et al.[20] have also found that at a special mixing ratio (x =1/3), $Na_4Sn_{1-x}Si_xS_4$ can form the same new phase in the space group of $I4_1/acd$. However, isovalent Tt-mixed $Na_4Sn_{0.67}Si_{0.33}S_4$ has a room-temperature conductivity of 1.23×10^{-2} mS cm^{-1}, too low to be of interest as a solid electrolyte. Only after introducing P^{5+}, the conductivity is enhanced to 1.6 mS cm^{-1} in $Na_{3.75}[Sn_{0.67}Si_{0.33}]_{0.75}P_{0.25}S_4$.[20]

In this work, we present a comprehensive study of the Na_3PnS_4-Na_4TtS_4 (Pn = P/As/Sb, Tt = Si/Ge/Sn) phase space of superionic conductors using density functional theory (DFT) calculations. We quantify the enthalpy for isovalent mixing, that is, P/Sb/As mixing, in tetragonal and cubic polymorphs of Na_3PnS_4, as well as the effect of such mixing on relative polymorph stability, electrochemical stability and moisture stability. We further extend our study to mixed $Na_{4-x}Tt_{1-x}Pn_xS_4$ phases, including the $Na_{11}Tt_2PnS_{12}$ archetype. We demonstrate that intrinsic electrochemical stability at both high and low voltages is limited by the least stable cation (whether Pn or Tt). Finally, a new composition $Na_{11}Sn_2AsS_{12}$ is proposed with potentially improved ionic conductivity as well as moisture stability over all previously reported compositions in this space.

2. Experimental Section

2.1. Structure Preparation

The archetypical crystal structures of the tetragonal and cubic forms of Na_3PnS_4 (t-Na_3PnS_4 and c-Na_3PnS_4, respectively),[6]

Dr. Z. Zhu, Dr. H. Tang, J. Qi, Dr. X.-G. Li, Prof. S. P. Ong
Department of NanoEngineering
University of California San Diego
9500 Gilman Dr, Mail Code 0448, La Jolla, CA 92093-0448, USA
E-mail: ongsp@eng.ucsd.edu

The ORCID identification number(s) for the author(s) of this article can be found under https://doi.org/10.1002/aenm.202003196.

DOI: 10.1002/aenm.202003196

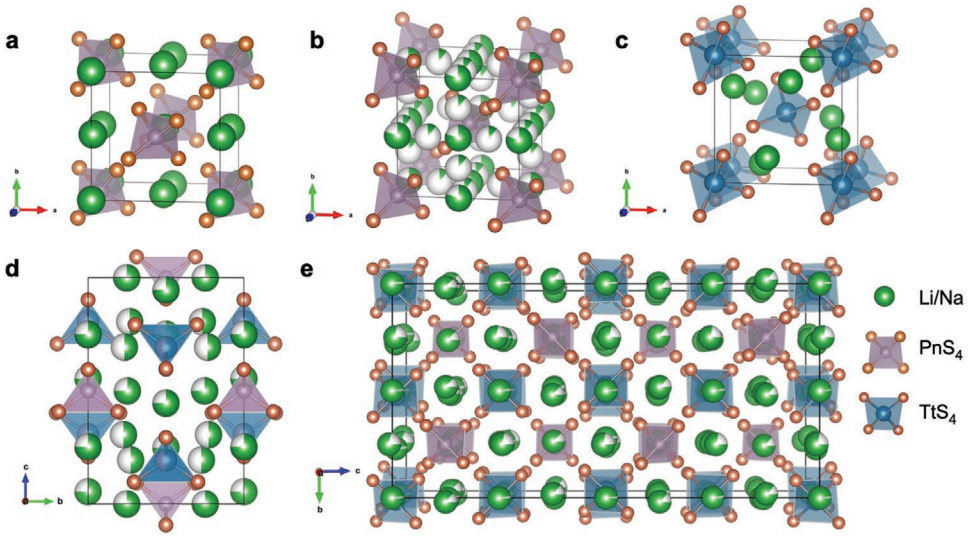

Figure 1. Crystal structures of a) tetragonal Na_3PnS_4 (space group: $P\bar{4}2_1c$), b) cubic Na_3PnS_4 (space group: $I\bar{4}3m$), c) Na_4TtS_4 (space group: $P\bar{4}2_1c$), d) $Li_{10}TtPn_2S_{12}$ (space group: $P4_2/nmc$), and e) $Na_{11}Tt_2PnS_{12}$ (space group: $I4_1/acd$). Purple tetrahedrons, PnS_4; blue tetrahedrons, TtS_4; green spheres, Li/Na.

Na_4TtS_4,[24] $Li_{10}TtPn_2S_{12}$,[25] and $Na_{11}Tt_2PnS_{12}$[18] are shown in **Figure 1**. The mixed compounds investigated in this work are listed in **Table 1** were generated in the following manner:

1. Isovalent mixed $Na_3Pn'_xPn''_{1-x}S_4$ (Pn′, Pn″ = P, As or Sb) structures with x in intervals of 1/16 were generated by enumerating all symmetrically distinct configurations[26] using a 2 × 2 × 2 supercell of t- and c-Na_3PnS_4. Although c-Na_3PnS_4 has partial occupancies in Na1 (6b, occ.=0.8) and Na2 (12d, occ. = 0.1) sites as experimentally reported,[6] the most stable configuration with fully occupied Na1 sites was employed for Pn′-Pn″ cation mixing.
2. Aliovalent mixed $Na_{4-x}Tt_{1-x}Pn_xS_4$ structures were generated by enumerating all symmetrically distinct Na vacancy/interstitial and Tt/Pn orderings in Na_3PnS_4 ($P\bar{4}2_1c$) and Na_4TtS_4 ($P\bar{4}2_1c$) supercells. It should be noted that only Na_4SnS_4[20] in this archetype was realized experimentally, and there were no reports of Na_4SiS_4 and Na_4GeS_4 in a similar structure. A Na_4SiS_4 phase was reported experimentally[27] but its structure was not adequately resolved. When x=1/4, 1/2, 3/4, 2×1×1 supercells were applied and 3 × 1 × 1 supercells were used for x = 1/3, 2/3. In addition, substitutions of different Tt and Pn in different ratios, charge balanced by modifications in Na concentration, were carried out on the primitive cell of $Na_{11}Tt_2PnS_{12}$ and conventional cell of $Li_{10}TtPn_2S_{12}$.

2.2. DFT Calculations

All DFT calculations were performed using the Vienna ab initio simulation package within the projector augmented-wave approach.[28,29] The Perdew–Burke–Ernzerhof generalized-gradient approximation (GGA) exchange-correlation functional[30] was used for all calculations.

For structural relaxations and energy calculations of the Na_3PnS_4-Na_4TtS_4 phases of primary interest, spin-polarized calculations were performing with an energy cutoff of 520 eV and a k-point density of at least 1000/(number of atoms were applied, similar to those used in the Materials Project (MP).[31] These energies were then combined with pre-computed energies for other phases in the MP for phase stability, moisture stability, and electrochemical stability analysis.

For ab initio molecular dynamics (AIMD) simulations, non-spin-polarized calculations were carried out with a smaller

Table 1. Compositions and structures investigated in this work. Cation species are Pn=P, As, Sb; Tt=Si, Ge, Sn.

Compound	Source (space group)	Mixing type	Mixing ratio (x)
$Na_3Pn'_xPn''_{1-x}S_4$	t-Na_3PnS ($P\bar{4}2_1c$)	Isovalent	x = 0, 1/16, 1/8, 3/16, 1/4, 5/16, 3/8,
	c-Na_3PnS_4 ($I\bar{4}3m$)		7/16, 1/2, 9/16, 5/8, 11/16, 3/4, 13/16,
			7/8, 15/16, 1
$Na_{4-x}Tt_{1-x}Pn_xS_4$	t-Na_3PnS_4 ($P\bar{4}2_1c$)	Aliovalent	x = 1/4, 1/3, 1/2, 2/3, 3/4
	Na_4TtS_4 ($P\bar{4}2_1c$)		x = 1/4, 1/3, 1/2, 2/3, 3/4
	$Na_{11}Tt_2PnS_{12}$ ($I4_1/acd$)		x = 1/4, 1/3, 1/2, 2/3, 3/4
	$Li_{10}TtPn_2S1_2$ ($P4_2/nmc$)		x = 1/3, 1/2, 2/3

plane-wave energy cutoff of 280 eV, a minimal Γ-centered $1 \times 1 \times 1$ k-point mesh. The time step was 2 fs. The AIMD simulations were performed in the *NVT* ensemble at six temperatures (800–1400 K or 700–1200 K depending on the temperatures at which Tt-S and/or Pn-S bond breaking was observed) with a Nose–Hoover thermostat,[32,33] with the volume (V) fixed as GGA-relaxed volume at 0 K, in line with typical approximations used in prior works.[34] At least 200 ps of AIMD simulations were performed to get reliable Na^+ ionic conductivity and activation energy. Framework trajectories were inspected at the highest temperatures (1400 K for $Na_{11}Sn_2PS_{12}$, 1200 K for $Na_{11}Sn_2AsS_{12}$, and $Na_{11}Sn_2SbS_{12}$) to ensure that the bonds (Tt—S, Pn—S) were not broken within the simulation temperatures.

All DFT and AIMD simulations were carried out using fully-automated workflows[35] built on the Python Materials Genomics (pymatgen)[36] library and Atomate scientific workflow package.[37,38]

2.3. Property Analysis

The 0K Na—Pn′—Pn″—S and Na—Tt—Pn—S phase diagrams were constructed by taking the convex hull of the energies of all phases in the respective compositional spaces.[39] From the 0K phase diagram, the energy above the convex hull (E_{hull}), an estimate of the phase stability, can be obtained for each phase of interest. In addition, the 0K pseudo-binary $Na_3Pn'S_4$-$Na_3Pn''S_4$ stability diagram were constructed for each Pn′-Pn″ combination, from which the mixing enthalpies of $Na_3Pn'_xPn''_{1-x}S_4$ can be obtained.

To estimate the electrochemical stability, the Na grand canonical phase diagrams[39] were constructed to determine the range of Na chemical potentials for which each solid electrolyte composition was stable against Na extraction or uptake, in line with the approach used in previous works[34,40] for analysis of alkali superionic conductors. In this approach, the SE/cathode and SE/anode interfaces were modeled as an open system where the SE was in contact with a Na sink at low Na chemical potential and Na source at high Na chemical potential, respectively.

The moisture sensitivity of each SE was estimated by the reaction energy of the SE with H_2O at 0K. This was done by constructing the Na—Pn′—Pn″—S—H—O or Na—Tt—Pn—S—H—O phase diagram and identifying the most exothermic reaction along the tie-line between the SE composition and H_2O.[34,41,42] The more negative the reaction energy, the more sensitive the SE was to moisture.

Finally, the diffusivity D of each SE at each AIMD simulation temperature was obtained by performing a linear fit of the mean square displacements of Na in the AIMD trajectories with time t, according to the following equation:

$$D = \frac{\left\langle [\Delta \mathbf{r}(t)]^2 \right\rangle}{2dt} \tag{1}$$

where $\Delta\mathbf{r}$ is the displacement of the diffusing Na atoms, and the dimensionality of diffusion $d = 3$ in this work. An Arrhenius plot was then constructed by plotting $\log(D)$ versus $1/T$, where T is the temperature, from which the activation barrier for conductivity and the extrapolated room-temperature conductivities and diffusivities can be obtained.

3. Results and Discussion

3.1. Polymorph Stability and Mixing Energies

3.1.1. Isovalent Cation Mixing in $Na_3Pn'_xPn''_{1-x}S_4$

The cubic lattice parameters of Na_3PnS_4 increase with the ionic radii of Pn^{5+}, from 7.048 Å for c-Na_3PS_4 to 7.253 Å for c-Na_3SbS_4. The relaxed structures and calculated E_{hull} are detailed in Table S1, Supporting Information. **Figure 2**a–c plot the energy difference between the cubic and tetragonal polymorphs, $E_{cubic}-E_{tetragonal}$, for $Na_3Pn'_xPn''_{1-x}S_4$. Though it has been established both computationally and experimentally[8,43–45] that there is no substantial difference in ionic conductivity between the tetragonal and cubic phases, $E_{cubic}-E_{tetragonal}$ provides a measure of the thermodynamic preference for one phase over the other. It may be observed that the tetragonal polymorph is more stable than the cubic polymorph by ≈3–6 meV atom^{-1} for all compositions. The energy differences between cubic and tetragonal polymorphs are very close for Na_3AsS_4 (3.5 meV atom^{-1}) and Na_3SbS_4 (4.3 meV atom^{-1}) and mixing of As or Sb into Na_3PS_4 tends to lead to a small relative stabilization of the cubic polymorph. The tetragonal-cubic phase transition is modulated in anion-mixed $Na_3PS_xSe_{4-x}$: Se-rich compositions with $x \leq 2$ have smaller $E_{cubic}-E_{tetragonal}$.[46] While $E_{cubic}-E_{tetragonal}$ decreases monotonically with x in $Na_3As_xP_{1-x}S_4$, the minimum of $E_{cubic}-E_{tetragonal}$ in $Na_3Sb_xAs_{1-x}S_4$ and $Na_3P_xSb_{1-x}S_4$ occurs at $x = 0.25$ and is slightly lower (<1 meV atom^{-1}) than the left end members in Figure 2b,c.

Figure 2d–f plot the mixing enthalpy for t-$Na_3Pn'_xPn''_{1-x}S_4$ (c-$Na_3Pn'_xPn''_{1-x}S_4$ see Figure S2, Supporting Information). Low mixing enthalpies (<kT≈ 25 meV atom^{-1} where k is the Boltzmann's constant and T = 300K) are observed between pairs of cations, with local minima observed at $x = 0.25$, 0.5, 0.75. P-As mixing leads to a small negative value of enthalpy of mixing (≈–1 meV per fu), which is in good agreement with previous studies.[16] The enthalpy for P-Sb mixing is the highest, which can be explained by the fact that P^{5+} and Sb^{5+} have the largest ionic radius difference between them. Though the energy differences between different Pn′-Pn″ orderings are generally small, we observe that the ground state orderings are the same for all mixing and compositions. For example, **Figure 3**a shows the ground state ordering for $Na_3As_{0.5}P_{0.5}S_4$, where PS_4 and AsS_4 tetrahedrons form alternating chains along the <110 > directions. The same ground state ordering is found for $Na_3Sb_{0.5}As_{0.5}S_4$ and $Na_3P_{0.5}Sb_{0.5}S_4$. Furthermore, complementary mixing compositions share the same ordering, that is, $Na_3As_{0.25}P_{0.75}S_4$ have the same ground state ordering as the $Na_3As_{0.75}P_{0.25}S_4$ structure shown in Figure 3b, but with the As and P atoms swapped. The space groups for the ground state orderings for $x = 0.25$, 0.5, 0.75 are *Cc*, *Pnc*2, and *Cc*, respectively. However, we note that the energy differences between different orderings are generally small and therefore, it is likely mixed phases are disordered

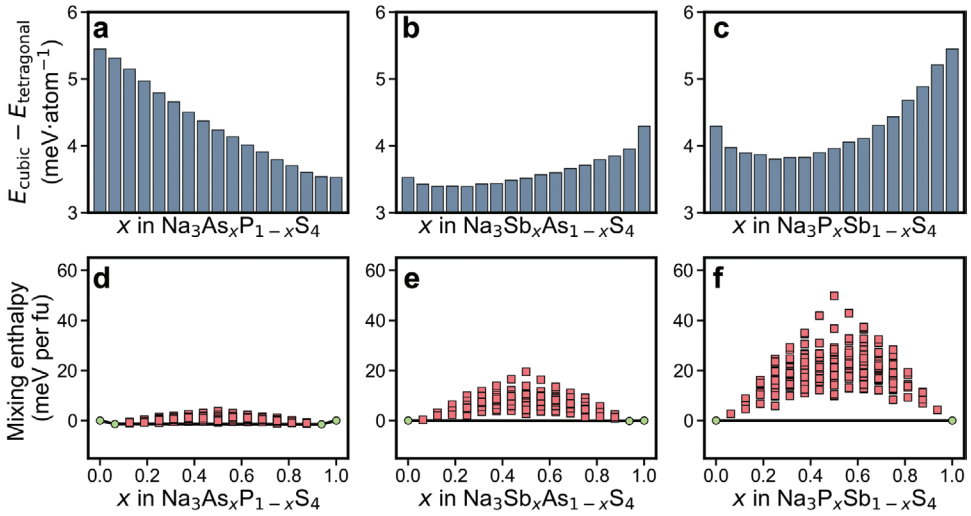

Figure 2. Polymorph stability and mixing enthalpy of $Na_3Pn'_xPn''_{1-x}S_4$ (Pn′,Pn″=P, As, Sb). a–c) Energy difference between the cubic and tetragonal phase (E_{cubic}–$E_{tetragonal}$) and d–f) mixing enthalpy of t-$Na_3Pn'_xPn''_{1-x}S_4$. Squares and circles markers are for unstable and stable structures, respectively. The mixed $Na_3Pn'_xPn''_{1-x}S_4$ systems are successively (from left to right): $Na_3As_xP_{1-x}S_4$, $Na_3Sb_xAs_{1-x}S_4$ and $Na_3P_xSb_{1-x}S_4$.

rather than exhibiting the symmetries of their ground state orderings.

3.1.2. Aliovalent Cation Mixing in $Na_{4-x}Tt_{1-x}Pn_xS_4$

Figure 4 compares the range in E_{hull} for different orderings in $Na_{4-x}Sn_{1-x}P_xS_4$ (x = 1/4, 1/3, 1/2, 2/3, 3/4) derived from different structure archetypes. It may be observed that the aliovalent-mixed structures derived from the recently discovered $Na_{11}Sn_2PS_{12}$ has the lowest energy among the four archetypes considered across the entire range of compositions. Interestingly, at x = 2/3, the $Li_{10}GeP_2S_{12}$ archetype have a very similar energy (within 1 meV atom^{-1}) as the $Na_{11}Sn_2PS_{12}$ archetype in their ground-state structures, which is consistent with the fact that $Na_{10}SnP_2S_{12}$ ($P4_2/nmc$) have been successfully synthesized experimentally.[4]

Figure 5 shows the E_{hull} of the ground state structure for all combinations of Tt and Pn at x = 1/4, 1/3, 1/2, and 3/4 in the $Na_{11}Tt_2PnS_{12}$-archetype. While the E_{hull} are relatively small (<8 meV atom^{-1}) for all mixing combinations, the lowest E_{hull} are observed at x = 1/3 for each Pn, with E_{hull} = 0 for Pn = P, As. This observation is consistent with the fact that $Na_{11}Sn_2PS_{12}$ and $Na_{11}Sn_2SbS_{12}$ (compositionally equivalent to x = 1/3) have already been synthesized experimentally. At this composition, the 16*e* sites are fully occupied by Tt and 8*a* sites are fully occupied by Pn. At any other compositions (x is not 1/3), such 16*e* and/or 8*a* sites will be occupied by two species, which leads to a higher E_{hull}. We test out this hypothesis by site swapping between 16*e* and 8*a* in $Na_{11}Sn_2SbS_{12}$. The cation-swapped structure is higher in energy (see Figure S5, Supporting Information) than the experimentally refined structure. The somewhat higher E_{hull} of the Sb-containing compounds can be attributed to the relatively large difference in ionic radius between Sb^{5+} and Si^{4+}/Ge^{4+} (see **Table 2**).

3.2. Moisture Stability

Figure 6 shows the computed reaction energies with water for isovalent mixed $Na_3Pn'_xPn''_{1-x}S_4$ and aliovalent-mixed $Na_{4-x}Tt_{1-x}Pn_xS_{12}$. It should be noted that only hydrolysis

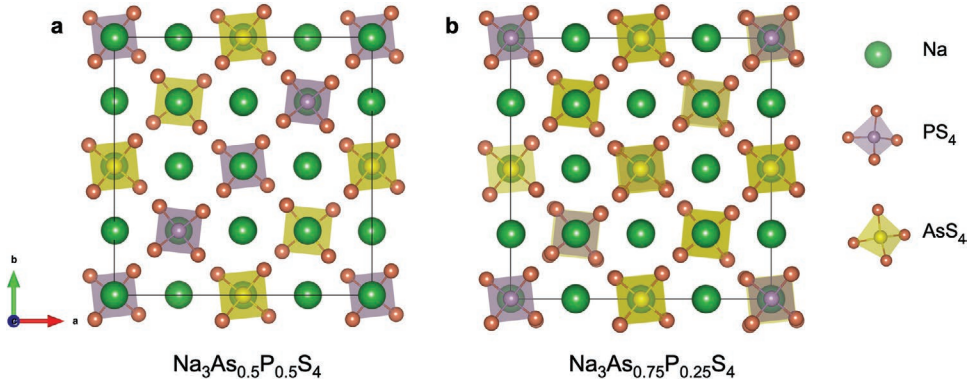

Figure 3. Ordering pattern (top view along *c* direction) of the most stable tetragonal structure for a) $Na_3As_{0.5}P_{0.5}S_4$ and b) $Na_3As_{0.75}P_{0.25}S_4$.

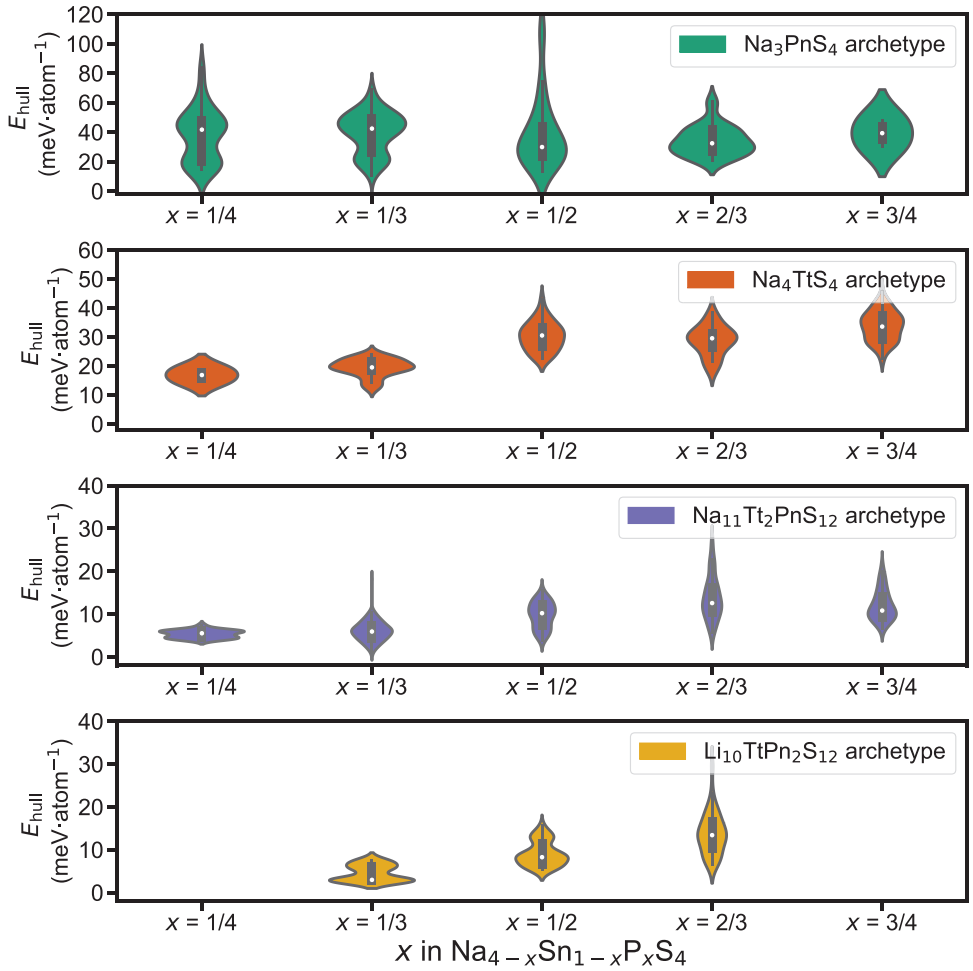

Figure 4. The range of energy above hull (E_{hull}) for different orderings of $Na_{4-x}Sn_{1-x}P_xS_4$. x = 1/4, 1/3, 1/2, 2/3, 3/4 for Na_3PnS_4, Na_4TtS_4, $Na_{11}Tt_2PnS_{12}$ archetypes and x = 1/3, 1/2, 2/3 for the archetype of $Li_{10}TtPn_2S_{12}$. The E_{hull} represents the energy difference with respect to the most stable decomposed products of Na_3PS_4 and Na_4SnS_4.

reactions are taken into account, and not hydration reactions (insertion of H_2O into the crystal). While we expect all the sulfides investigated to be reactive with water to some extent, hydration has generally been shown to be less detrimental than hydrolysis to the stability and performance of these materials.[47,48] The corresponding reaction energies and products are given in Tables S3 and S4, Supporting Information. The reactivity of $Na_3P_xSb_{1-x}S_4$ with H_2O is the highest among all $Na_3Pn'_xPn''_{1-x}S_4$ systems. NaS_2 and Na_3SbS_3 are formed in the Sb-rich region (x = 0.0625–0.375), Na_2S_5, t-Na_3PS_4 appear at moderate P-Sb mixing ratios (x = 0.4375), and Na_2S_5 and H_2S (gaseous phase at room temperature) form in the P-rich region (x = 0.5625–0.9375). The sharp decrease in moisture stability with P/Sb mixing can be attributed to the high mixing energies as shown in Figure 2. In contrast, $Na_3As_xP_{1-x}S_4$ compounds are predicted to be more stable against H_2O with a less negative reaction energy. This observation is consistent with previous experimental and computational studies of Na_3AsS_4.[15,16] The $Na_3Sb_xAs_{1-x}S_4$ compositions (zero reaction energy with H_2O) as shown in Figure 6a show no thermodynamically favorable hydrolysis reactions will occur with the products such as H_2S. Based on our DFT calculations, Sb-As mixing is less reactive with H_2O than the other two pairs, especially than Sb-P mixing.

For quaternary $Na_{4-x}Tt_{1-x}Pn_xS_{12}$ compounds (Figure 6b), it may be observed that the Tt species rather than Pn elements determine the moisture stability, with Si < Ge < Sn in order of increasing moisture stability, that is, less negative reaction energy with H_2O. Si-containing compounds are by far the least stable, due to the formation of highly stable SiO_2 upon reaction with H_2O. When Tt is not Si, the aqueous stability is determined by Pn and follows the same trend as in isovalent $Na_3Pn'_xPn''_{1-x}S_4$, that is, P-containing compositions are less stable than Sb/As.

3.3. Electrochemical Stability

Figure 7 and Table S2, Supporting Information show the predicted electrochemical window (EW) of selected pure and mixed Na_3PnS_4/Na_4TtS_4 as well as $Na_{11}Tt_2PnS_{12}$ calculated using the grand potential phase diagram approach.[39] It should be noted that the predicted EW of Na_3AsS_4 of 1.57–2.47 V is substantially larger than the 1.94–2.12 V reported earlier by the current

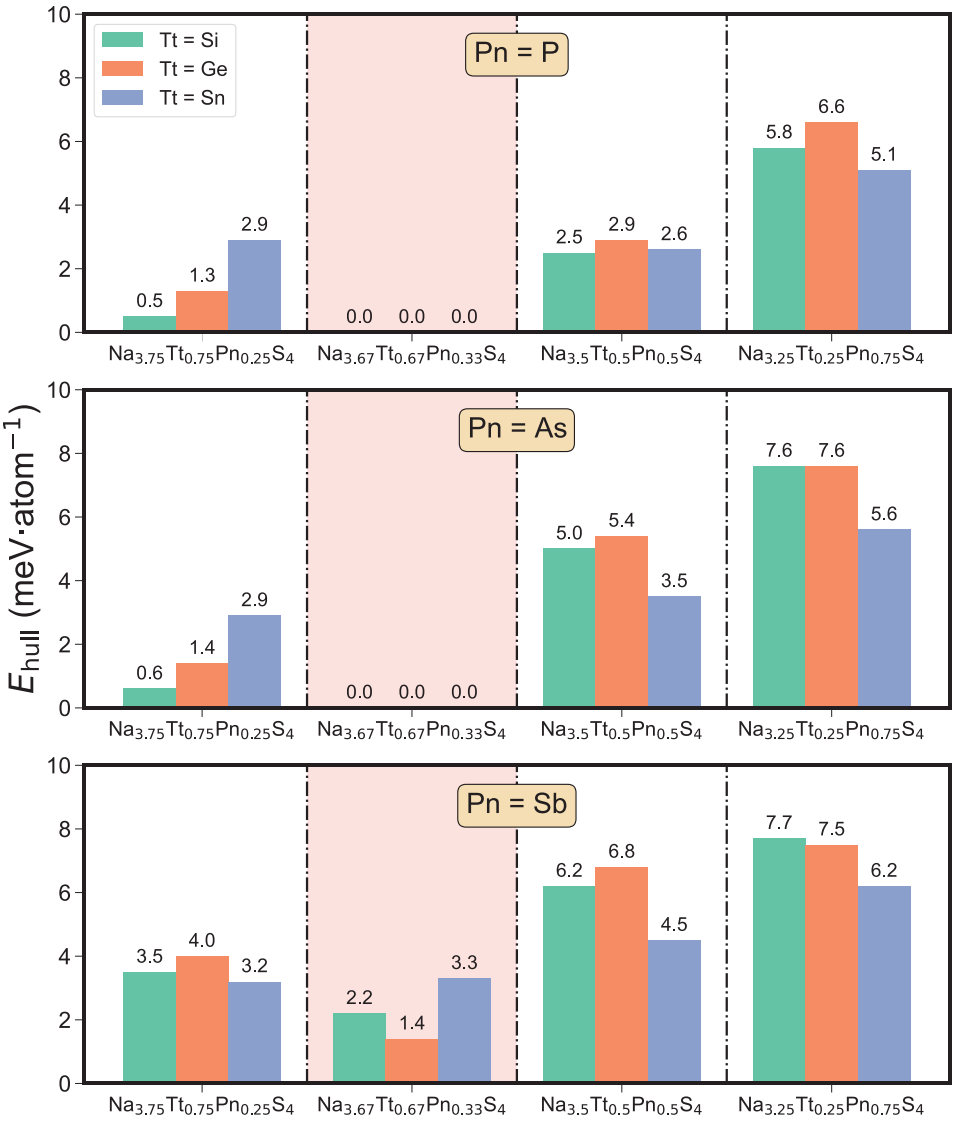

Figure 5. Thermodynamic stability of $Na_{4-x}Tt_{1-x}Pn_xS_4$(x = 1/4, 1/3, 1/2, 3/4). The most energy favorable composition is at x = 1/3 (equivalent to $Na_{11}Tt_2PnS_{12}$) as shown in coral-shaded region.

authors.[49] This is due to the Na_3AsS_4 phase being not present in the previous work. The electrochemical reactions products of pure and mixed Na_3PnS_4 and Na_4TtS_4 at different potentials are given in Supporting Information (Figures S6 and S7, Supporting Information).

Table 2. Shannon ionic Radii of cation species in tetrahedral coordination investigated in this work.[23]

Element	Oxidation State	Ionic Radius [Å]
Si	4+	0.26
Ge	4+	0.39
Sn	4+	0.55
P	5+	0.17
As	5+	0.34
Sb	5+	0.6

From Figure 7, it may be observed that the EW for a mixed composition is governed by the least electrochemically stable component phase at both the cathodic (high voltage) and anodic (low voltage) limits. For example, the EW of $Na_3As_{0.5}Sb_{0.5}S_4$ is bounded by Na_3SbS_4 at the cathodic limit and Na_3AsS_4 at the anodic limit. The decomposed products of mixed compositions within EW ranges and beyond anodic/cathodic limits are presented in Figures S6d–f and S7d–f, Supporting Information. Similarly, the EW of $Na_{11}Ge_2SbS_{12}$ (1.52–2.07V) is bounded by Na_4GeS_4 (1.05–2.06V) at the cathodic limit and Na_3SbS_4 (1.54–2.35V) at the anodic limit. Furthermore, a general observation can be made that all the Na_4TtS_4 phases have lower cathodic and anodic limits than the Na_3PnS_4 phases, which imply that the EW of any mixed Na_4TtS_4-Na_3PnS_4 phase would be bounded by Na_4TtS_4 at the cathodic limit and Na_3PnS_4 at the anodic limit. The result is that mixed Na_4TtS_4-Na_3PnS_4 would have a much smaller EWs than either the Na_3PnS_4 and Na_4TtS_4 phase (see Figure 7c).

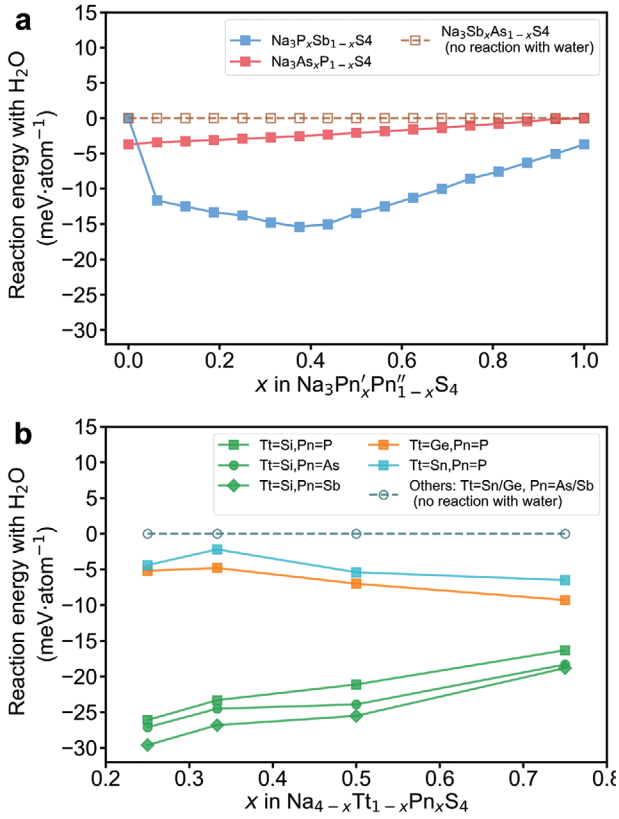

Figure 6. Reaction energies with H_2O at 0K for a) $Na_3Pn'_xPn''_{1-x}S_4$ and b) $Na_{4-x}Tt_{1-x}Pn_xS_{12}$. The zero reaction energies indicate compounds ($Na_3Sb_xAs_{1-x}S_4$ in $Na_3Pn'_xPn''_{1-x}S_4$ and Tt = Sn/Ge, Pn = As/Sb in $Na_{4-x}Tt_{1-x}Pn_xS_{12}$) are predicted to be stable against moisture (shown in unfilled markers linked by dashed lines). Compounds that are predicted to react with water (reaction energies <0 meV atom^{-1}) are shown in filled markers linked by solid lines.

3.4. Ionic and Electronic Conductivity

Given the poor moisture stability of Si phase and high cost of Ge, we selected the Sn-containing $Na_{11}Sn_2PnS_{12}$ (Pn = P, As, Sb) for further studies of their ionic conductivities using AIMD simulations and electronic band gap using HSE calculations.

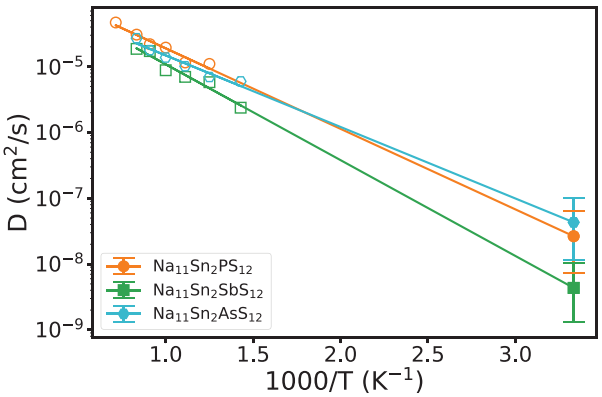

Formula	σ_{300K} (mS·cm^{-1})	Error range of σ_{300K} (mS·cm^{-1})	E_a (eV)	E_g (eV)
$Na_{11}Sn_2PS_{12}$	2.77	[1.99, 3.85]	0.243±0.028	2.53
$Na_{11}Sn_2AsS_{12}$	4.52	[3.31, 6.17]	0.216±0.027	2.62
$Na_{11}Sn_2SbS_{12}$	0.45	[0.31, 0.64]	0.289±0.031	2.50

Figure 8. (Top) Arrhenius plots for $Na_{11}Sn_2PnS_{12}$ (Pn=P, As, Sb) obtained from AIMD simulations. Unfilled markers indicate the operation temperatures at which we run AIMD calculations, while filled markers with error bars are the extrapolated room temperature of 300 K. (Bottom) Na^+ conductivity at 300 K (σ_{300K}), error range of σ_{300K}, activation energy (E_a) obtained from AIMD simulations as well as HSE band gap (E_g) of $Na_{11}Sn_2PnS_{12}$ (Pn=P, As, Sb).

Figure 8 shows the Arrhenius plots for $Na_{11}Sn_2PnS_{12}$ (Pn = P, As, Sb) in an *NVT* ensemble at six temperatures (see Experimental Section for details). The extrapolated room temperature Na^+ conductivities are 2.77 mS cm^{-1} for $Na_{11}Sn_2PS_{12}$, 4.52 mS cm^{-1} for $Na_{11}Sn_2AsS_{12}$, and 0.45 mS cm^{-1} for $Na_{11}Sn_2SbS_{12}$. The Na^+ conductivities of $Na_{11}Sn_2PS_{12}$ and $Na_{11}Sn_2SbS_{12}$ are in excellent agreement with experimental results ($Na_{11}Sn_2PS_{12}$: 1.4–3.7 mS cm^{-1}[18,19];$Na_{11}Sn_2SbS_{12}$: 0.2–0.56 mS cm^{-1}[21,22]). The error ranges of σ_{300K}, D_{300K}, and E_a from unweighted and weighted linear regression scheme[50] are shown in Supporting Information (see Table S5, Supporting Information). The estimated activation energies (E_a) for 0.24 eV for $Na_{11}Sn_2PS_{12}$ and 0.29 eV for $Na_{11}Sn_2SbS_{12}$ are also in good agreement with previously reported experimental values of 0.25[18] and 0.34 eV,[22] respectively. We note that the ionic conductivity of $Na_{11}Sn_2AsS_{12}$ is predicted to be on a similar order

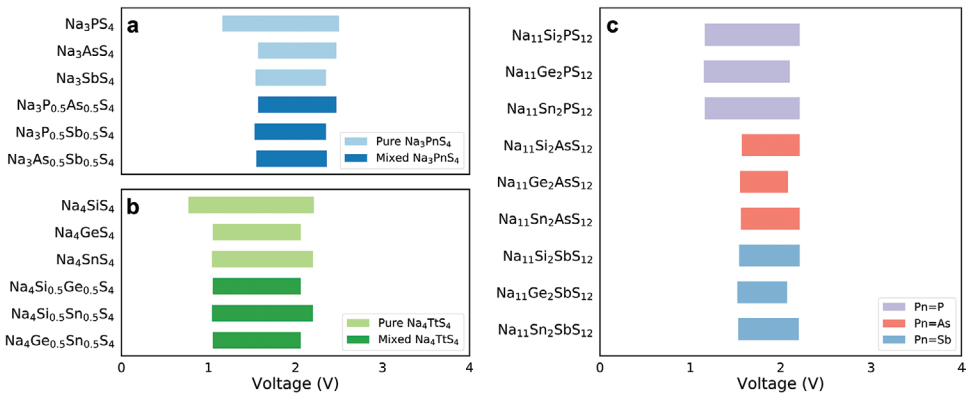

Figure 7. Electrochemical windows of a) Na_3PnS_4 and $Na_3Pn'_xPn''_{1-x}S_4$, b) Na_4TtS_4, and $Na_4Tt'_{0.5}Tt''_{0.5}S_4$ c) $Na_{11}Tt_2PnS_{12}$ where Pn = P, As, Sb, and Tt = Si, Ge, Sn.

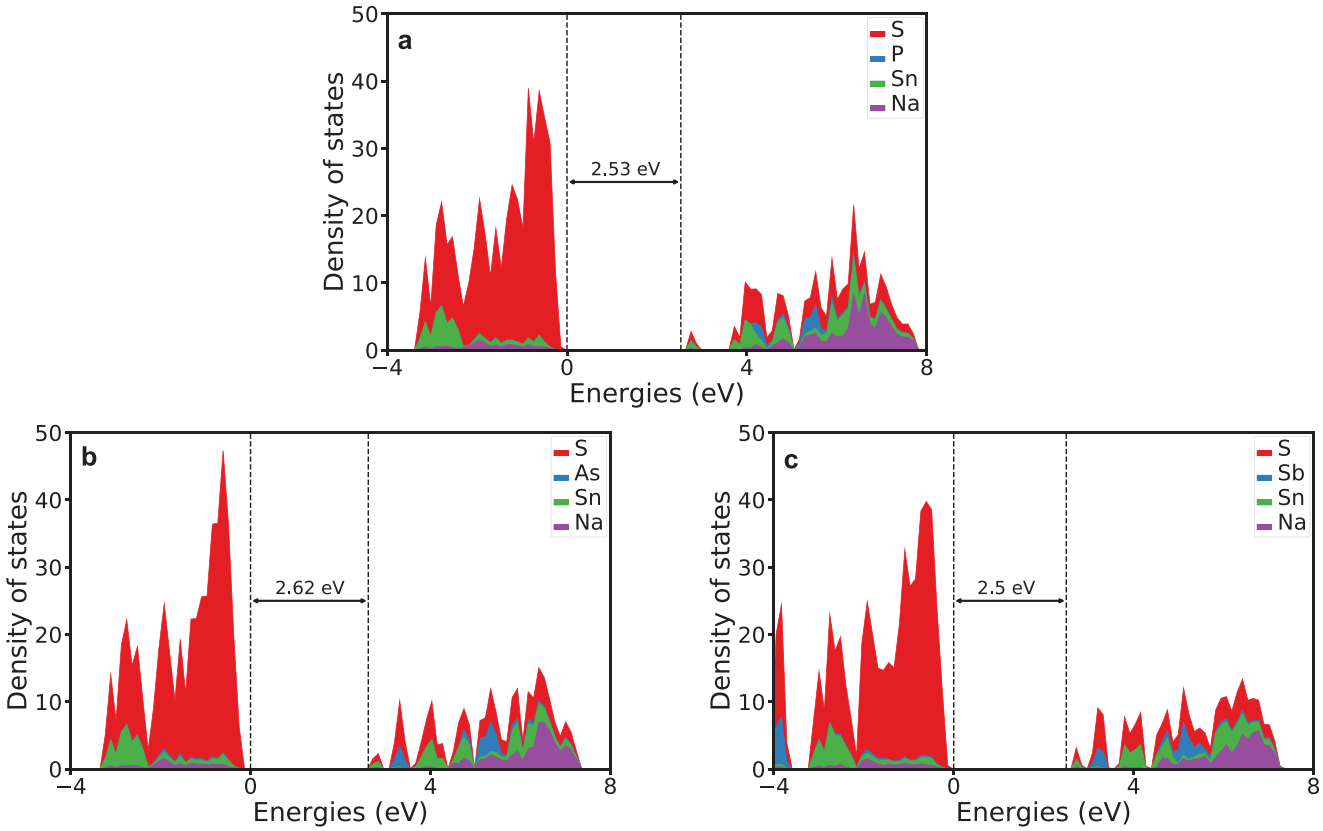

Figure 9. Calculated element-projected density of states (DOS) for a) $Na_{11}Sn_2PS_{12}$ (band gap E_g = 2.53 eV) b) $Na_{11}Sn_2AsS_{12}$ (E_g = 2.62 eV) and c) $Na_{11}Sn_2SbS_{12}$ (E_g = 2.5 eV) using the HSE06 screened hybrid functional.

as $Na_{11}Sn_2PS_{12}$ (>1 mS cm^{-1}), one order of magnitude higher than $Na_{11}Sn_2SbS_{12}$. We hypothesize this is because the ionic radius of As^{5+} (60 pm) is closer to that of P^{5+} (52 pm) than Sb^{5+} (74 pm).

Figure 9 shows the calculated densities of states (DOS) for $Na_{11}Sn_2PnS_{12}$ using HSE functional. All of the three candidates are relatively large and similar band gaps of ≈2.5–2.62 eV. This is due to the fact that the valence band maximums in these materials are dominated by S-*p* electrons, and the conduction band minimums are dominated by hybridized Sn and S orbitals. The calculated DOS for other Na_3PnS_4 and Na_4TtS_4 are given in Figures S8 and S9, Supporting Information.

4. Conclusion

To conclude, we have comprehensively investigated the Na_3PnS_4-Na_4TtS_4 (Pn = P/As/Sb, Tt = Si/Ge/Sn) phase space of superionic conductors in terms of key SE performance metrics such as phase stability, moisture stability, ionic conductivity, and electronic conductivity. From DFT calculations, we show that isovalent Pn′-Pn″ mixing is generally favorable (low mixing enthalpies) in the Na_3PnS_4 structure. Aliovalent Tt—Pn mixing, on the other hand, exhibits a clear preference for the recently discovered $Na_{11}Tt_2PnS_{12}$ archetype, and to a slightly lesser extent, the $Li_{10}TtPn_2S_{12}$ archetype.

Aliovalent Tt—Pn mixing offers an invaluable lever to tune Na^+ conductivity (through control of Na concentration) as well as moisture stability. The presence of small, highly charged "hard" cations such as Si^{4+} and P^{5+} results in poor moisture stability, and their substitution with larger, softer cations such as Ge^{4+}, Sn^{4+}, Sb^{5+}, and As^{5+} decreases the reactivity with water. However, the major compromise from Tt—Pn mixing comes in terms of the electrochemical stability. We establish that the electrochemical window that is set by the less electrochemically stable species at both the anodic limit (set by the Pn^{5+} species) and cathodic limits (set by the Tt^{4+} species), and these limits in fact narrow with an increase in cation sizes. Among the compositions investigated, $Na_{11}Sn_2AsS_{12}$ is predicted to be a hitherto unexplored SE with a combination of high Na^+ conductivity of 4.52 mS cm^{-1}, exceeding that of the previously studied $Na_{11}Sn_2PS_{12}$ and $Na_{11}Sn_2SbS_{12}$, as well as good moisture stability. However, it is predicted to have a relatively narrow electrochemical window given approximately by the overlap in electrochemical window stability of the Na_3AsS_4 and Na_4SnS_4 end members, and the toxicity of As is also a potential concern. Nevertheless, $Na_{11}Sn_2AsS_{12}$ can still a promising SE if its narrower electrochemical window is mitigated, for example, through electrode/SE buffer layers.[51–53]

Supporting Information

Supporting Information is available from the Wiley Online Library or from the author.

Acknowledgements

This work was supported by the Energy & Biosciences Institute through the EBI-Shell program contract number PT78832. The authors also acknowledge computational resources provided by the Triton Shared Computing Cluster (TSCC) at the University of California, San Diego, and the Extreme Science and Engineering Discovery Environment (XSEDE) supported by National Science Foundation under grant no. ACI-1053575.

Conflict of Interest

The authors declare no conflict of interest.

Keywords

AIMD, cation mixing effect, DFT, moisture stability, sodium solid electrolytes

Received: October 7, 2020
Revised: December 7, 2020
Published online:

[1] J. B. Goodenough, H. Y.-P. Hong, J. A. Kafalas, *Mater. Res. Bull.* **1976**, *11*, 203.
[2] H. Y.-P. Hong, *Mater. Res. Bull.* **1976**, *11*, 173.
[3] X. Lu, G. Xia, J. P. Lemmon, Z. Yang, *J. Power Sources* **2010**, *195*, 2431.
[4] W. D. Richards, T. Tsujimura, L. J. Miara, Y. Wang, J. C. Kim, S. P. Ong, I. Uechi, N. Suzuki, G. Ceder, *Nat. Commun.* **2016**, *7*, 11009.
[5] M. Jansen, U. Henseler, *J. Solid State Chem.* **1992**, *99*, 110.
[6] A. Hayashi, K. Noi, A. Sakuda, M. Tatsumisago, *Nat. Commun.* **2012**, *3*, 856.
[7] A. Hayashi, K. Noi, N. Tanibata, M. Nagao, M. Tatsumisago, *J. Power Sources* **2014**, *258*, 420.
[8] Z. Zhu, I. H. Chu, Z. Deng, S. P. Ong, *Chem. Mater.* **2015**, *27*, 8318.
[9] R. P. Rao, H. Chen, L. L. Wong, S. Adams, *J. Mater. Chem. A* **2017**, *5*, 3377.
[10] I.-H. Chu, C. S. Kompella, H. Nguyen, Z. Zhu, S. Hy, Z. Deng, Y. S. Meng, S. P. Ong, *Sci. Rep.* **2016**, *6*, 33733.
[11] X. Feng, P.-H. Chien, Z. Zhu, I.-H. Chu, P. Wang, M. Immediato-Scuotto, H. Arabzadeh, S. P. Ong, Y.-Y. Hu, *Adv. Funct. Mater.* **2019**, *29*, 1807951.
[12] A. Banerjee, K. H. Park, J. W. Heo, Y. J. Nam, C. K. Moon, S. M. Oh, S. T. Hong, Y. S. Jung, *Angew. Chemie., Int. Ed.* **2016**, *55*, 9634.
[13] L. Zhang, D. Zhang, K. Yang, X. Yan, L. Wang, J. Mi, B. Xu, Y. Li, *Adv. Sci.* **2016**, *3*, 1600089.
[14] H. Wang, Y. Chen, Z. D. Hood, G. Sahu, A. S. Pandian, J. K. Keum, K. An, C. Liang, *Angew. Chem., Int. Ed.* **2016**, *55*, 8551.
[15] Z. Yu, S. L. Shang, J. H. Seo, D. Wang, X. Luo, Q. Huang, S. Chen, J. Lu, X. Li, Z. K. Liu, D. Wang, *Adv. Mater.* **2017**, *29*, 1605561.
[16] S. L. Shang, Z. Yu, Y. Wang, D. Wang, Z. K. Liu, *ACS Appl. Mater. Interfaces* **2017**, *9*, 16261.
[17] A. Hayashi, N. Masuzawa, S. Yubuchi, F. Tsuji, C. Hotehama, A. Sakuda, M. Tatsumisago, *Nat. Commun.* **2019**, *10*, 5266.
[18] Z. Zhang, E. Ramos, F. Lalère, A. Assoud, K. Kaup, P. Hartman, L. F. Nazar, *Energy Environ. Sci.* **2018**, *11*, 87.
[19] M. Duchardt, U. Ruschewitz, S. Adams, S. Dehnen, B. Roling, *Angew. Chem., Int. Ed.* **2018**, *57*, 1351.
[20] H. Jia, Y. Sun, Z. Zhang, L. Peng, T. An, J. Xie, *Energy Storage Mater.* **2019**, *23*, 508.
[21] J. W. Heo, A. Banerjee, K. H. Park, Y. S. Jung, S. T. Hong, *Adv. Energy Mater.* **2018**, *4*, 4.
[22] E. P. Ramos, Z. Zhang, A. Assoud, K. Kaup, F. Lalère, L. F. Nazar, *Chem. Mater.* **2018**, *30*, 7413.
[23] B. Shannon, *Acta Cryst.* **1976**, *A32*, 751.
[24] J.-C. Jumas, E. Philippot, F. Vermot-Gaud-Daniel, M. Ribes, M. Maurin, *J. Solid State Chem.* **1975**, *14*, 319.
[25] N. Kamaya, K. Homma, Y. Yamakawa, M. Hirayama, R. Kanno, M. Yonemura, T. Kamiyama, Y. Kato, S. Hama, K. Kawamoto, A. Mitsui, *Nat. Mater.* **2011**, *10*, 682.
[26] G. L. W. Hart, R. W. Forcade, *Phys. Rev. B* **2008**, *77*, 224115.
[27] N. Tanibata, K. Noi, A. Hayashi, M. Tatsumisago, *RSC Adv.* **2014**, *4*, 17120.
[28] P. E. Blöchl, *Phys. Rev. B* **1994**, *50*, 17953.
[29] G. Kresse, J. Furthmüller, *Phys. Rev. B* **1996**, *54*, 11169.
[30] J. P. Perdew, K. Burke, M. Ernzerhof, *Phys. Rev. Lett.* **1996**, *77*, 3865.
[31] A. Jain, S. P. Ong, G. Hautier, W. Chen, W. D. Richards, S. Dacek, S. Cholia, D. Gunter, D. Skinner, G. Ceder, K. A. Persson, *APL Mater.* **2013**, *1*, 011002.
[32] S. Nosé, *J. Chem. Phys.* **1984**, *81*, 511.
[33] W. G. Hoover, *Phys. Rev. A* **1985**, *31*, 1695.
[34] S. P. Ong, Y. Mo, W. D. Richards, L. Miara, H. S. Lee, G. Ceder, *Energy Environ. Sci.* **2012**, *6*, 148.
[35] Z. Deng, Z. Zhu, I.-H. Chu, S. P. Ong, *Chem. Mater.* **2017**, *29*, 281.
[36] S. P. Ong, W. D. Richards, A. Jain, G. Hautier, M. Kocher, S. Cholia, D. Gunter, V. L. Chevrier, K. A. Persson, G. Ceder, *Comput. Mater. Sci.* **2013**, *68*, 314.
[37] A. Jain, S. P. Ong, W. Chen, B. Medasani, X. Qu, M. Kocher, M. Brafman, G. Petretto, G.-M. Rignanese, G. Hautier, D. Gunter, K. A. Persson, *Concurrency Comput.: Pract. Exper.* **2015**, *27*, 5037.
[38] K. Mathew, J. H. Montoya, A. Faghaninia, S. Dwarakanath, M. Aykol, H. Tang, I.-h. Chu, T. Smidt, B. Bocklund, M. Horton, J. Dagdelen, B. Wood, Z.-K. Liu, J. Neaton, S. P. Ong, K. Persson, A. Jain, *Comput. Mater. Sci.* **2017**, *139*, 140.
[39] S. P. Ong, L. Wang, B. Kang, G. Ceder, *Chem. Mater.* **2008**, *20*, 1798.
[40] Y. Mo, S. P. Ong, G. Ceder, *Chem. Mater.* **2012**, *24*, 15.
[41] Y. Zhu, X. He, Y. Mo, *J. Mater. Chem. A* **2016**, *4*, 3253.
[42] I.-H. Chu, H. Nguyen, S. Hy, Y.-C. Lin, Z. Wang, Z. Xu, Z. Deng, Y. S. Meng, S. P. Ong, *ACS Appl. Mater. Interfaces* **2016**, *8*, 7843.
[43] S. Takeuchi, K. Suzuki, M. Hirayama, R. Kanno, *J. Solid State Chem.* **2018**, *265*, 353.
[44] T. Krauskopf, S. P. Culver, W. G. Zeier, *Inorg. Chem.* **2018**, *57*, 4739.
[45] T. Famprikis, Ö. U. Kudu, J. A. Dawson, P. Canepa, F. Fauth, E. Suard, M. Zbiri, D. Dambournet, O. J. Borkiewicz, H. Bouyanfif, S. P. Emge, S. Cretu, J.-N. Chotard, C. P. Grey, W. G. Zeier, M. S. Islam, C. Masquelier, *J. Am. Chem. Soc.* **2020**, *142*, 18422.
[46] S.-H. Bo, Y. Wang, G. Ceder, *J. Mater. Chem. A* **2016**, *4*, 9044.
[47] Y. Zhu, Y. Mo, *Angew. Chem., Int. Ed.59*, 17472.
[48] Y. Tian, Y. Sun, D. C. Hannah, Y. Xiao, H. Liu, K. W. Chapman, S.-H. Bo, G. Ceder, *Joule* **2019**.
[49] H. Tang, Z. Deng, Z. Lin, Z. Wang, I.-H. Chu, C. Chen, Z. Zhu, C. Zheng, S. P. Ong, *Chem. Mater.* **2018**, *30*, 163.
[50] X. He, Y. Zhu, A. Epstein, Y. Mo, *npj Comput. Mater.* **2018**, *4*, 1.
[51] A. Banerjee, H. Tang, X. Wang, J.-H. Cheng, H. Nguyen, M. Zhang, D. H. S. Tan, T. A. Wynn, E. A. Wu, J.-M. Doux, T. Wu, L. Ma, G. E. Sterbinsky, M. S. D'Souza, S. P. Ong, Y. S. Meng, *ACS Appl. Mater. Interfaces* **2019**, *11*, 43138.
[52] Y. Xiao, Y. Wang, S.-H. Bo, J. C. Kim, L. J. Miara, G. Ceder, *Nat. Rev. Mater.* **2020**, *5*, 105.
[53] T. Nakamura, K. Amezawa, J. Kulisch, W. G. Zeier, J. Janek, *ACS Appl. Mater. Interfaces* **2019**, *11*, 19968.